Research Article Open Access

Umar Daraz[1,2], Tariq Mahmood Ansari[1,*], Shafique Ahmad Arain[3], Muhammad Adil Mansoor[2,4] and Muhammad Mazhar[2,5]

Study of solvent effect on structural and photoconductive behavior of ternary chalcogenides $InBiS_3$-In_2S_3-Bi_2S_3 composite thin films deposited via AACVD

https://doi.org/10.1515/mgmc-2019-0011
Received September 23, 2018; accepted April 03, 2019.

Abstract: In the present work ternary composite $InBiS_3$-In_2S_3-Bi_2S_3 (IBS) thin films are developed using a homogeneous mixture of precursors $[Bi(S_2CN(C_2H_5)_2)_3]_2$ **(1)** and $[In(S_2CNCy_2)_3]\cdot 2py$ **(2),** separately in toluene and chloroform solutions at 500°C under an inert atmosphere of argon gas *via* aerosol assisted chemical vapor deposition (AACVD) technique. The phase purity, chemical composition and morphological study of both the films deposited from toluene and chloroform solutions are characterized by X-ray diffraction (XRD), X-ray photoelectron spectroscopy (XPS), Raman spectroscopy and Field emission scanning electron microscopy (FESEM). The surface morphology showed rod like structure of the films developed from toluene while the films grown from chloroform solution give flake like shapes. The UV-visible spectroscopy explicated that the thin films developed from toluene and chloroform solutions show wide range absorption in whole visible region. Linear Scan voltammetry results show that both the films give negligible dark current, however, the films fabricated from toluene solution give a sharp steep curve with maximum photocurrent density of 2.3 $mA\cdot cm^{-2}$ at 0.75 V vs Ag/AgCl/3M KCl using 0.05 M sodium sulphide solution under AM 1.5 G illumination (100 $mW\cdot cm^{-2}$), while the film grown from chloroform generates a photocurrent density of 2.1 $mA\cdot cm^{-2}$ under similar conditions. The LSV outcomes are further supported by electrochemical impedance spectroscopy (EIS) that gives charge transfer resistance (R_{ct}) value of 8,571 Ω for the films developed from toluene as compared to films fabricated from chloroform with R_{ct} value of 12,476 Ω.

Keywords: $InBiS_3$-In_2S_3-Bi_2S_3; thin film; chalcogenides; band gap; photocatalysts

1 Introduction

It is well established fact all over the world that natural energy sources are at decrepit (Banos et al., 2011). In the 21st century there has been a paradigm shift from conventional methods of energy resources to clean and sustainable modes of energy generation categorize as renewable energy (Ellabban et al., 2014; Tong et al., 2012) and in this regard photocatalytic technology is the top choice for scientists (Chen et al., 2016). These photocatalysts can produce hydrogen by photolysis of water and also destroy pollutants by converting them into carbon dioxide and water at room temperature and pressure using sunlight (Protti et al., 2014; Wang et al., 2014). The two most important photocatalysts used in the past 40 years are metal sulphides and metal oxides, the latter being mostly activated by ultraviolet radiations. The UV radiation constitute only 3-5% of total

*** Corresponding author: Tariq Mahmood Ansari,** Institute of Chemical Sciences, Bahauddin Zakariya University, Multan 60800, Pakistan, e-mail: tariqansari@bzu.edu.pk
Umar Daraz, Institute of Chemical Sciences, Bahauddin Zakariya University, Multan 60800, Pakistan; Department of Chemistry, Faculty of Science, University of Malaya, 50603, Kuala Lumpur, Malaysia
Shafique Ahmad Arain, Institute of Chemistry, Shah Abdul Latif University Khairpur, Sindh, Pakistan
Muhammad Adil Mansoor, Department of Chemistry, Faculty of Science, University of Malaya, 50603, Kuala Lumpur, Malaysia; Department of Chemistry, School of Natural Sciences (SNS), National University of Science and Technology, H-12, Islamabad, Pakistan
Muhammad Mazhar, Department of Chemistry, Faculty of Science, University of Malaya, 50603, Kuala Lumpur, Malaysia; Department of Environmental Sciences, Fatima Jinnah Women University, The Mall, Rawalpindi, Pakistan

solar spectrum that is why an efficient photocatalysts are needed that can effectively use all visible and UV portion of the sunlight (Chen et al., 2015; Dong et al., 2015; Primo et al., 2011). Metal sulphides, therefore, are best choice for scientists due to better visible and UV radiation response and of suitable band gap energy value for photocatalytic water splitting (Tsuji et al., 2005). Various metal sulphides are reported as semiconductors and photocatalysts in past (Kudo and Miseki, 2009; Shen et al., 2012). But the other aspect of metal sulphide semiconductors is that these are relatively unstable and undergo photocorrosion very rapidly. This is due to high susceptibility of sulphide ions to undergo oxidation as compared to H_2O, resulting in the leaching of metal ions. However, it can be avoided to some extent by coupling with some wide gape semiconductors or inorganic matrix and by using sacrificial reagents (Na_2S or Na_2SO_3) as electrolytes (Ning et al., 2017; Weide et al., 2016; Zhang and Guo, 2013).

Low band gap values i.e. 1.2-1.7 eV, high absorbance co-efficient, environmental harmony and ease of conversion of solar light energy to electrical energy (~5%) make bismuth sulphide a promising material for photoelectrical applications in comparison to other chalcogenide semiconductors (Dunst et al., 2016; Liufu et al., 2007). The chemical stability and effect of nanostructure on photoelectric performance also renders bismuth sulphide suitable for photoconducting behavior when exposed to sunlight and used as photoelectrode (Tahir et al., 2010). Based upon above mentioned grounds, bismuth sulphides with uniformly distributed nano particles have been tailored in the last few decades for their active utilization as photosensitive sources (Khadraoui et al., 2016; Madoun et al., 2013; Pineda et al., 2012; Haaf et al., 2013). On the other hand, indium based chalcogenides are also attractive solid materials due to their extensive use especially in photovoltaics, optoelectronic and many technological applications (Bhira et al., 2000; Sankir et al., 2015; Yadav and Salunke, 2015). This is possibly due to their compact structure, flexibility in band gap values and photoconductive nature (Bhira et al., 2000).

The indium sulphide based solar cells are not only non-toxic but also improves the light transmission in the blue wavelength region on having wide band gap than that of CdS (Calixto et al., 2005; Nagesha et al., 2001). As aforementioned that the bismuth sulphide and indium sulphide can efficiently convert light energy to electrical energy (Chen et al., 2008; Haaf et al., 2013; Moreno et al., 2011; Sterner et al., 2005), therefore, the blending of indium sulphide with bismuth sulphide can thus leads to a new composite with improved optoelectronic behavior and photovoltaic applications (Ali et al., 2018).

The photocatalytic response of thin films also depends on the connectivity and uniform distribution of particles on the surface of substrate. The selection of technique for thin films fabrication is of great importance as structure of these films is strongly influenced by the methodology adopted for their fabrication. Several techniques have been used for metal thin films fabrication (Ali et al., 2018; Cheon et al., 1997; Huang et al., 2016; Jinlong et al., 2016; Liu et al., 2003; Madeswaran et al., 2003; Zou et al., 2017), however believing on our preceding skills, we picked solution dependent aerosol assisted chemical vapour deposition (AACVD) technique. The solution based AACVD is a fast, low in cost, reproducible and scalable technique and furnished thin films of high purity, uniform surface and adhesive nature (Marchand et al., 2013). The microstructure of films can easily be controlled by tuning deposition parameters (Munawar et al., 2017). Herein, we report first time, the deposition of $InBiS_3$-In_2S_3-Bi_2S_3 (IBS) composite thin films on FTO substrate at 500°C from mixture of precursors $[Bi(S_2CN(C_2H_5)_2)_3]_2$ **(1)** and $[In(S_2CNCy_2)_3]\cdot 2py$ **(2)** using two different solvents, toluene and chloroform via AACVD.

2 Results and discussion

The role of physicochemical properties such as viscosity, boiling point, enthalpy of combustion of the solvent, size of the aerosol droplet, temperature of deposition and nature of the substrate etc. has significant effect on shape and size, porosity and morphology of the particles that influence photoelectric behaviour of the thin films. The homogenous and heterogeneous decomposition mechanism in thin film deposition process is also directly associated with all these factors. In the present work we evaluated the impact of these factors on morphology and photoelectric behaviour IBS composite thin films.

The IBS composite films are developed for 40 min from equimolar homogenous solutions of precursors **(1)** and **(2)** in toluene and chloroform solvents in separate experiments on FTO substrate at 500°C *via* AACVD. The synthesized films showed outstanding stability towards air and moisture. The morphology of thin films prepared from two different solvents was compared by FESEM analysis. The films developed from toluene solvent that have boiling point, evaporation and combustion enthalpies of 110.6°C, 38.064 kJ/mol -3910.3 kJ/mol respectively, presented nanowires of IBS composite on FTO substrate. Whereas,

the films developed from chloroform solvent having boiling point, evaporation and combustions enthalpies of 61.15°C, 29.4 kJ/mol and -473.21 kJ/mol respectively, gave petal like arrangement of IBS composite. The thickness of IBS films as determined by profilometer suggest 390 nm and 410 nm thick layers in case of toluene and chloroform solvents respectively.

2.1 X-Rays diffraction studies

Figure 1 shows the X-ray diffraction patterns of IBS thin films developed from homogenous solution of precursors **(1)** and **(2)** in toluene and chloroform at 500°C *via* AACVD. The reflections obtained show that the IBS thin film constitutes three distinct phases of $InBiS_3$, Bi_2S_3 and In_2S_3, out of which the first two belong to orthorhombic while third phase has cubic crystal system. The peaks labelled by (■) at 2θ value of 22.45, 23.89, 32.00, 33.08, 36.86, 39.27 and 45.68° corresponds to lattice planes of (103), (011), (302), (204), (114), (205) and (206) respectively of $InBiS_3$. Sticky pattern matching is available in Figure S1. While the reflections indicated by (+) at 2θ value of 15.88, 17.91, 25.21, 28.84, 40.13, 46.71 and 52.82° reflects lattice planes (200), (210), (310), (320), (411), (501) and (312) respectively of orthorhombic bismuth sulphide (Bi_2S_3).

The lattice reflections observed at 2θ values of 25.21, 27.43, 28.84, 34.19, 51.51, 59.25° indicated by (●) in Figure 1 are in close agreement with lattice planes of (300), (311), (222), (410), (610) and (444) of In_2S_3The peaks labelled by (▼) in both of the IBS composite films are originated due to FTO substrate. The XRD reflections obtained from toluene and chloroform solutions not only lie at same positions but also provide sharp peak referring high crystallinity. Moreover, the crystallite size by Scherer's calculator was estimated about 128 and 160 nm at 2θ value for IBS composite films fabricated from toluene and chloroform respectively. However, for a better insight into crystallinity and morphology, FESEM studies were performed.

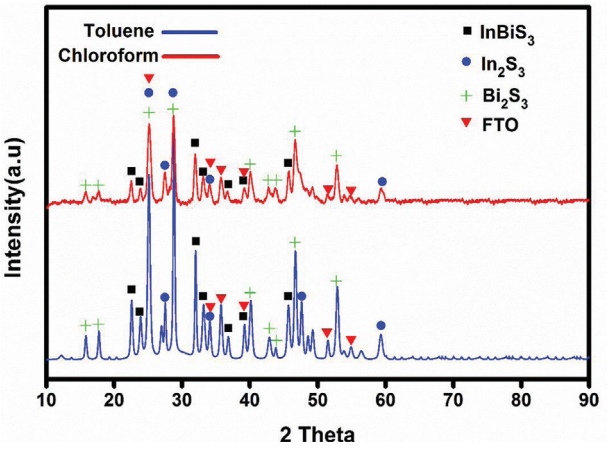

Figure 1: XRD pattern of $InBiS_3$-In_2S_3-Bi_2S_3 composite thin films fabricated on FTO substrate at 500°C from homogenous solutions of precursors **(1)** and **(2)** in toluene (blue) and chloroform (red).

2.2 XPS analysis

The chemical composition of the deposited $InBiS_3$-In_2S_3-Bi_2S_3 composite thin films and oxidation state of individual elements were evaluated by X-ray photoelectron spectroscopy (XPS) that is in good match with phase analysis of XRD output as depicted in Figure 2. The survey scan spectra (Figure 2a) of the films prepared from precursors solution of toluene (red) and chloroform (blue) confirm the presence of all the elements in expected ratio of 1:1:3 for in: Bi:S.

The high-resolution spectrum of the bismuth (Figure 2b) discloses a 4f doublet state at binding energies of 158.4 eV and 163.7 eV, for the Bi $4f^7$ and $4f^5$, respectively, for Bi_2S_3. These absorption bands with separation energy of 5.3 eV correspond to +3 oxidation states of Bi in Bi_2S_3 (Grigas et al., 2002). The component peaks at 159.2 and 164.6 eV in narrow scan of Bi are assigned to FTO glass substrate and remaining relatively low intensity peaks are correlated with $InBiS_3$ representing its small concentration in the end product (Ali et al., 2018). The peak appeared at binding energy of 161.15 eV is due to sulphur (S2p) in sulphide state (Ananthoju et al., 2014; Yang et al., 2014). Similarly, the high-resolution spectrum of indium also provides doublet states at binding energies 444.7 eV and 452.5 eV corresponding to In $3d^5$ and In $3d^3$, respectively (Figure 2c).

The deconvolution of In high resolution spectrum also provides a component peak at 442.4 eV which emerged due to FTO glass substrate (Ku et al., 2016). The S 2p core level spectrum with peak position at 161.1 eV is shown in Figure 2d. It is well reported that a single peak in between 160 and 164 eV for sulphur is due to its sulphide phase, which is confirmed in present results.

2.3 Raman spectroscopy

The fabricated IBS thin films were subjected to Raman spectroscopical analysis to evaluate the structural blueprints at micro level. The Raman spectra of IBS thin films developed from toluene and chloroform solutions are depicted in Figure S4. There appear seven distinct

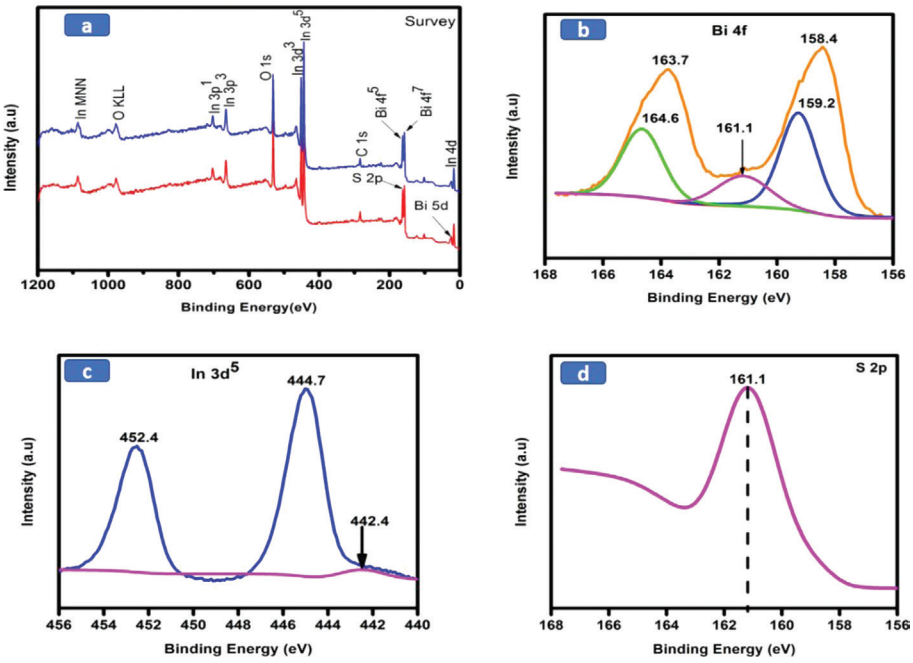

Figure 2: XPS spectra of $InBiS_3$-In_2S_3-Bi_2S_3 thin films developed from precursors **(1)** and **(2)** using toluene and chloroform as solvents at 500°C; (a) survey scan, (b) narrow scan of bismuth, (c) narrow scan of indium and (d) narrow scan of sulphur.

vibrational modes in IBS composite thin films developed from toluene solution of precursors **1** and **2**. The vibrational modes observed at 250 and 370 cm^{-1} are in close match with the reported pure phase of In_2S_3 (Spasevska et al., 2012) whereas the modes at 184, 277 and 965 cm^{-1} belongs to pure phase Bi_2S_3 (Ota and Srivastava, 2007; Pathak, 2013; Rabin et al., 2006). The vibrational modes observed at 151.6 and 525 cm^{-1} are due to the contribution of FTO substrate (Berengue et al., 2010). The low frequency vibrational mode observed at 225 cm^{-1} showed the slight deviation from reported Raman shift of Bi_2S_3 (237 cm^{-1}) (Zumeta et al., 2014) and this possibly credited to the synergic effect of indium and bismuth sulphide. The Raman spectra of IBS composite thin films developed from chloroform solution depicted the same pattern but vibrational modes are of relatively low intensities. This difference in Raman spectra of IBS composite thin films in two different solvents can be explained on the basis of FESEM analysis where films developed from toluene solution showed more uniform distribution of nanowires and offer more exposed surface area as compared to petal like arrangement of films particles in chloroform solvent.

2.4 Morphological studies

The morphological studies of as deposited $InBiS_3$-In_2S_3-Bi_2S_3 composite thin films were accomplished by using field emission scanning electron microscopy (FESEM) and results are depicted in Figure 3. The IBS thin films fabricated by using toluene solution of precursors **(1)** and **(2)** present well connected nano wire possessing uniform distribution which persists over entire FTO substrate (Figures 3a and 3b). These nanowires vary in size from several micrometers (μm) to nanometers (nm) in length and width respectively as measured in high magnified FESEM image (Figure S5). This compact arrangement of nano wires may help the movement of electrons throughout the structure once stimulated by sunlight and consequently better conduction can be observed.

Whereas IBS films generated from chloroform solution of **1** and **2** afford vertical growth of particles in the form of wafers or sharp petals of flowers (Figures 3c and 3d). The dimensions of these wafers are also in nanometers and possess well defined boundaries as shown in Figure S6. Apparently, the vertically grown wafers are developing a uniform texture, however, at the base of these petals some discrete particles are visible. Indeed, morphology of an electrode is one of the key factors to determine the efficiency of electrode in terms of light harvesting capability as well as its interaction with electrolyte. Therefore, the vertically grown wires from toluene solution arranged in a cris-cross fashion can provide better surface area to interact with electrolyte from top to bottom. It is believed that the thin film chemistry involves homogeneous and heterogeneous reactions when

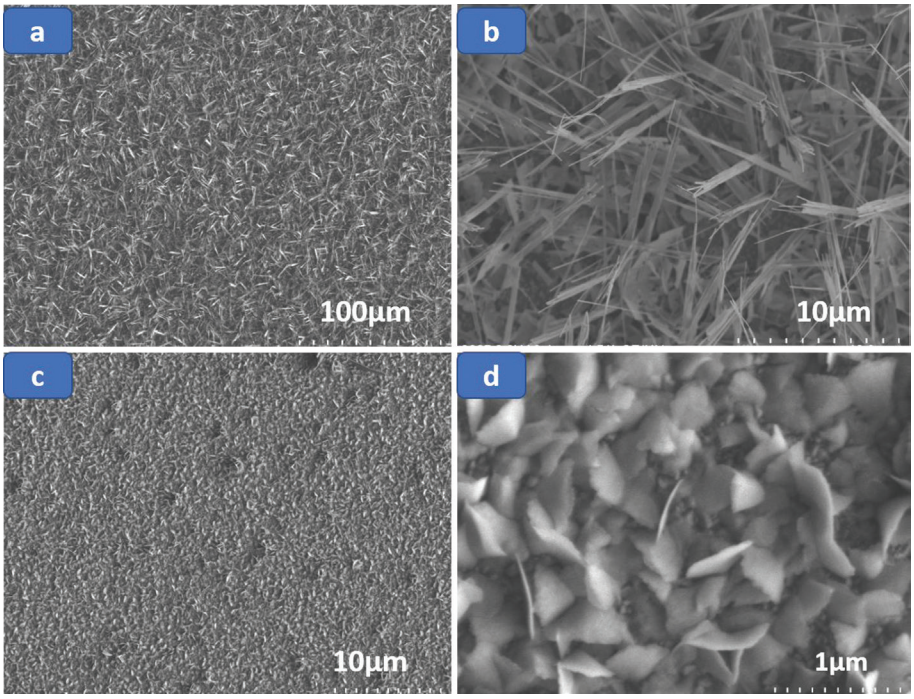

Figure 3: SEM images of $InBiS_3$-In_2S_3-Bi_2S_3 composite thin films deposited on FTO substrate using toluene solvent (a) low magnification and (b) high magnification, in chloroform low magnification (c) and the (d) high magnification at temperature of 500°C.

developed from AACVD technique. The possibility of homogeneous or heterogeneous decomposition process highly depends on certain physical parameters like boiling points, densities, surface tension along with enthalpies of combustion of the solvents used during fabrication process. Low boiling solvent having more enthalpy of combustion involves homogenous phenomenon during films formation in contrast to high boiling solvent of low combustion enthalpy which gives thin films through heterogeneous mechanism (Mansoor et al., 2017a; Munawar et al., 2017). It has been observed that the film formation from toluene solution was influenced by both the homogeneous and heterogeneous process thus decomposition of precursors and their vertical growth in the form of nanowires occur simultaneously. While, owing to low boiling point and high heat of combustion, precursor solution of chloroform preferably undergoes homogenous reaction leading to petal like structure with more voids and least exposed surface area.

2.5 Optical studies

The UV-Vis spectra of the composite $InBiS_3$-In_2S_3-Bi_2S_3 thin films synthesized from toluene and chloroform solutions was recorded in range of 380-780 nm. It is apparent that both the films show wide range absorption that gradually increases towards lower wavelength region as shown in Figures 4a and 4b. The optical band gap of IBS composite thin films is determined by the Tauc's equation (Mansoor et al., 2017b).

$$\alpha h\nu = A\,(h\nu - E_g)^{\gamma} \tag{1}$$

where α is the linear absorption coefficient of the material, $h\nu$ is the photon energy, A is a proportionality constant and γ is a constant depending on the band gap nature; $\gamma = 1/2$ for allowed direct band gap and $\gamma = 2$ for indirect band gap. The direct band gap was calculated by using Tauc's equation arranged as $(\alpha h\nu)^2 = A_1(h\nu - E_g)$. A plot of $(\alpha h\nu)^2$ versus $h\nu$ gave a linear region with slope A_1 whose extrapolation to $\alpha(h\nu) = 0$ would yield the direct band gap values of 1.42, 1.78 and 2.00 eV for individual components $InBiS_3$, Bi_2S_3 and In_2S_3 respectively in IBS composite thin films fabricated at 500°C from toluene solution (Inset of Figure 4a). Whereas, the IBS composite films developed from chloroform solution has band gap energy values of 1.51, 1.84 and 2.02 eV for distinctive components $InBiS_3$, Bi_2S_3 and In_2S_3 respectively (Inset of Figure 4b). The reported band gap value is 1.3-2.2 eV for $InBiS_3$, (Ali et al., 2018; Kale and Lokhande, 2005), 1.8-1.85 eV for Bi_2S_3 (Tahir et al., 2010) and 2.2 eV for In_2S_3 (Ehsan et al., 2013). The values of band gap for IBS composite thin films in toluene solution is less than that of films developed

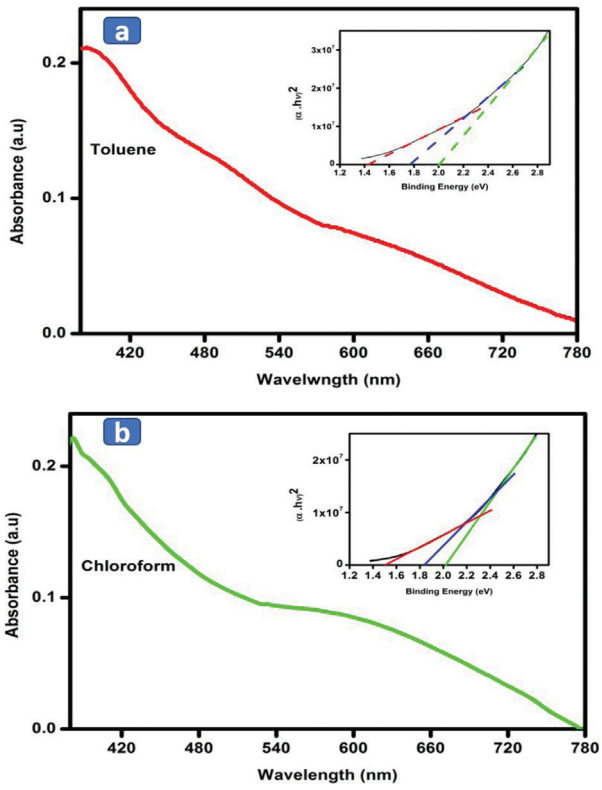

Figure 4: UV visible spectra of IBS films fabricated from (a) toluene (b) chloroform, insets are respective Tauc's plot indicating band gaps of individual components.

from chloroform solution. It is believed that this shift in band gaps is due to uniform distribution, porosity and more exposed surface area of nanowires formed from toluene solution that result in better electronic excitation and reducing electron-hole recombination. As the films prepared from chloroform has petal like structure, less porous and therefore the inner surface is not completely exposed, thus most probably the covered surface does not actively participate in light absorptions and electron excitations. Moreover, toluene solution gives nano wires of thickness 390 nm in contrast to petal shaped IBS growth of thickness 410 nm in chloroform solution.

2.6 Photoelectrochemical studies

The photoelectrochemical measurements of IBS composite thin film synthesised from toluene and chloroform solutions were performed in 1.5 sun illumination applying three-electrodes electrochemical work station using thin film as an anode, Platinum wire as cathode and Ag/AgCl in 3 M KCl as reference electrode. Both the IBS electrodes fabricated in toluene and chloroform exhibited an anodic

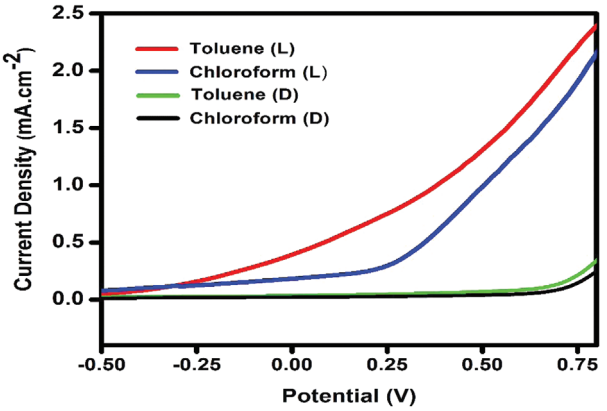

Figure 5: Linear sweep voltammetry (LSV) of $InBiS_3$-In_2S_3-Bi_2S_3 thin films developed from precursors **(1)** and **(2)** using toluene and chloroform as solvents at 500°C via AACVD.

photocurrent which gradually increases with the increase of anodic bias (Figure 5). It is observed that the dark current from both the films is negligible. However, under illumination the films fabricated from toluene solution gives a sharp steep with maximum photocurrent density of 2.3 mA·cm^{-2} at 0.75 V, while the films fabricated from chloroform solution show an onset potential at 0.23 V after which it gives a sharp rise in photocurrent density with maximum value of 2.1 mA·cm^{-2} at 0.75 V. The better exposure of surface area from the connected bunch of nanowires not only facilitates electrode-electrolyte interaction but also reduces the electron-hole recombination.

The maximum photocurrent achieved before saturation point, in the case of previously reported works on synthesis of individual In_2S_3 and Bi_2S_3 thin films using AACVD technique, was 1.5 mA·cm^{-2} and 1.9 mA·cm^{-2} respectively (Ali et al., 2018; Ehsan et al., 2013; Tahir et al., 2010). But in the present work, the photoresponse of IBS composite thin films developed in toluene starts below 0 potential and gives a photocurrent density of 400 μA·cm^{-2} at 0.00 V which reaches to maximum value of 2.3 mA·cm^{-2} without reaching saturation point. This shows improvement in comparison to the previously reported works where the photoactivity is effective with applied potential. Apart from homogeneous distribution of particles it is expected that there exists synergic interaction between In_2S_3 and Bi_2S_3 that tend to induce high photocurrent density (without applied potential) by reducing charge-hole recombination and high charge transfer mechanism. While, it is believed that due to least exposed surface of agglomerates between the petals grown from chloroform solution, electronic transfer is reduced as compared to the thin film grown from toluene solution and thus produces a low photocurrent at low potential.

However, with the applied potential photocurrent density grown from the chloroform films give a steep rise at an onset potential of 0.25 V. Therefore, we conclude that the photocurrent in the chloroform film is dependent on applied bias that activates the inner layers reducing loss of charge carriers in voids and pinholes.

The electrochemical impedance spectroscopic characterization was carried out to understand the interfacial charge transfer resistance inside the surface of electrodes and electrolyte. Figure 6 shows the Nyquist plots of the IBS thin films fabricated from toluene and chloroform under dark and illumination. The intersections of the high frequencies semicircles at the real axis signify the equivalent series resistance of the test material (R_s). The R_s values under illumination for both the films are tabulated as Table 1. It is found that under dark conditions both the films show a part of bigger semicircle, while under illumination, there is formation of small half semicircles followed by curves tilted towards imaginary axis.

It is also noticed that the thin films developed from toluene solution gives smaller region of semicircle and also the vertical line more towards imaginary axis as compared to the film prepared from chloroform solution (Figure 7). This observation also supports better conductive behaviour of film fabricated from toluene solution where it gives less charge transfer resistance (R_{ct}) value of 8,571 Ω as compared to film fabricated from chloroform with R_{ct} value of 12,476 Ω. This suggests that there is least electronic recombination in the film fabricated from toluene. These findings are further supported by bode phase plot (Figure 8). The low and middle frequencies peaks characterise the diffusion inside the electrolyte and the electron transportation in the semiconductors. The maximum frequencies (ω_{max}) in the middle frequency region of the Bode phase plots for both the IBS thin films under illumination condition are given in Table 1. Because ω_{max} is inversely associated with the electron lifetime ($\tau_n = 1/(2\pi\omega_{max})$), a decrease in the ω_{max} indicates a reduced rate for the charge-recombination process. It is noteworthy the IBS thin film from toluene solution exhibited longest $\tau_{n,}$ under illumination as compared to IBS (chloroform)

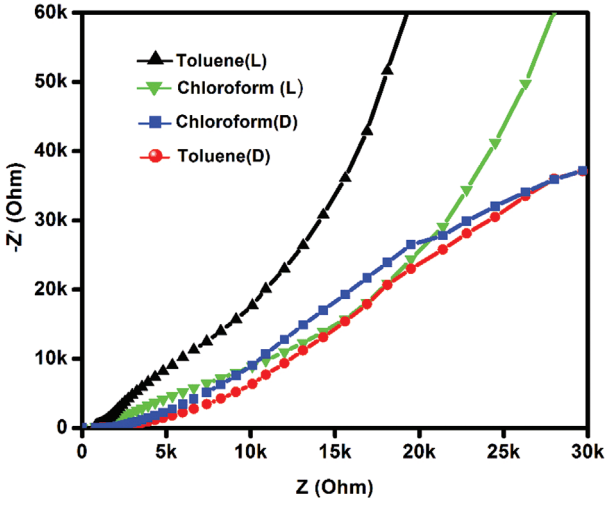

Figure 6: Nyquist plot of IBS thin films developed from homogeneous solution of precursors **(1)** and **(2)** in toluene and chloroform under illumination and without illumination.

Table 1: EIS results of IBS composite thin films indicating values of R_s, R_{ct}, ω_{max} and τ_n.

Sample (illumination)	R_s (Ohm)	R_{ct} (Ohm)	ω_{max} (Hz)	τ_n (ms)
IBS (toluene)	624.2	8571	0.2964	0.537
IBS (chloroform)	0.97	12476	0.5097	0.312

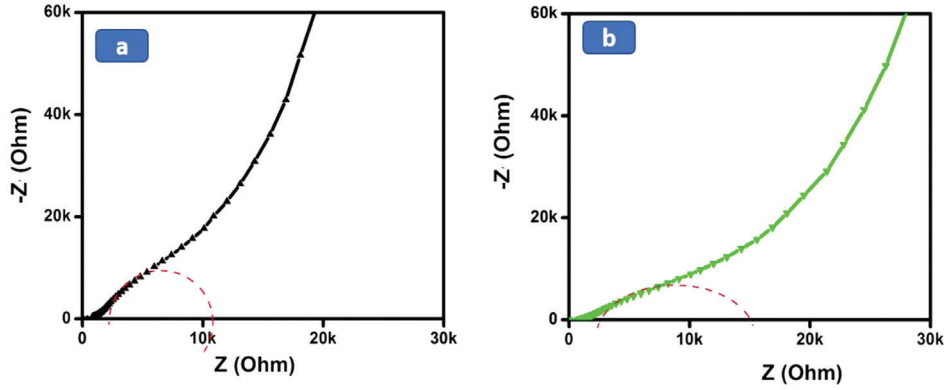

Figure 7: Semicircles of Nyquist plot for the films developed from (a) toluene and (b) chloroform under illumination.

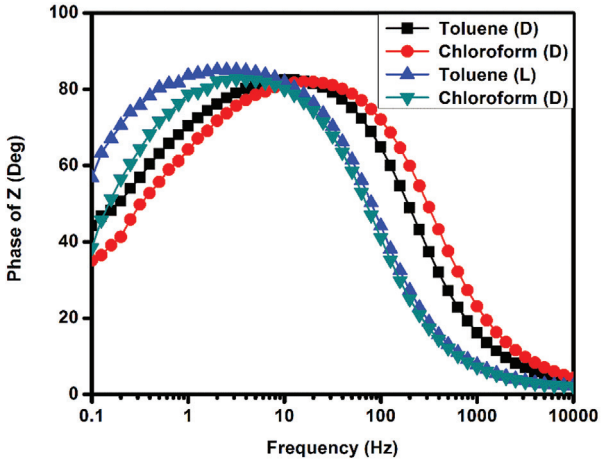

Figure 8: Bode phase plot of IBS thin films developed from homogenous solution of precursors **(1)** and **(2)** in toluene and chloroform under illumination and dark conditions.

which indicated that the electrons survived from the recombination process. Consequently, it is concluded that due to longer electron lifetime (τ_n) and low charge transfer resistance (R_{ct}), the IBS thin films fabricated from toluene solution displayed improved photocurrent density. The above-mentioned discussion convinces effective utilization of IBS composite thin films in solar cell applications and photolytic splitting of water as well.

In summary, these principal outcomes demonstrated that the IBS composite thin films exhibited much improved photoconductive behavior as compared to the previously deposited individual thin films of In_2S_3 and Bi_2S_3. The choice of the solvent for desired surface morphology results in upgrading photocurrent density with improved electron life time and reduced charge transfer resistance when using toluene as solvent.

3 Conclusion

The IBS composite thin films are successfully fabricated on FTO substrate at 500°C from dual source precursors $[Bi(S_2CN(C_2H_5)_2)_3]_2$ **(1)** and $[In(S_2CNCy_2)_3]\cdot 2py$ **(2),** having similar thermal properties using two different solvents i.e. toluene and chloroform by aerosol assisted chemical vapor deposition technique and used as photoelectrode. The comparative study of the thin films deposited in two different solvents show well connected nanowires developed from toluene solution and possess a band gap of 1.82 eV and provide improved photocurrent density of 2.3 mA·cm^{-2} at applied potential of 0.75 V as compared to flake shaped thin films developed from chloroform solution studied under similar conditions that have band gap value of 1.96 eV and current density 2.1 mA·cm$^{-2.}$ The impedance studies in terms of Nyquist curves further reinforced the superiority of nanowires and offer less charge transfer resistance value 8,571 Ω as compared to petal shaped thin films with R_c value than 12,476 Ω. These results indicate that depositions parameters influence morphology, shape and structure of the deposited films and also affect the photochemical activity.

Experimental

Synthesis of $[Bi(S_2CN(C_2H_5)_2)_3]_2$ (1) and $[In(S_2CNCy_2)_3]\cdot 2py$ (2)

The precursor complexes $[Bi(S_2CN(C_2H_5)_2)_3]_2$ **(1)** and $[In(S_2CNCy_2)_3]\cdot 2py$ **(2)** were synthesized following the reported procedures by the reaction of potassium dithiocarbamate with bismuth nitrate in acetone (Tahir et al., 2010) and sodium dithiocarbamate with indium chloride in methanol (Ehsan et al., 2013). The precursors **(1)** and **(2)** were characterized by melting point, elemental analysis and FTIR spectroscopical analysis. Details of synthetic procedures and characterizations are given in Supporting information.

Deposition of thin films by AACVD

The deposition of $InBiS_3$-In_2S_3-Bi_2S_3 composite thin films was carried out on fluorine doped tin oxide (FTO) by dual source using homogenous solution of precursors **(1)** and **(2)** in toluene and chloroform solvents in separate experiments at 500°C applying aerosol assisted chemical vapor deposition (AACVD) technique (Mansoor et al., 2014). Before deposition experiment, the substrate materials (FTO glass) having length of 25.4 mm, width 12.7 mm and diameter of 2.2 mm with surface resistance 7 Ω/sq. were subjected to ultrasonic cleaning with ethanol and acetone and finally rinsed with distilled water. In a typical procedure, 0.360 g (0.303 mmol) of $[Bi(S_2CN(C_2H_5)_2)_3]_2$ **(1)** and 0.316 g (0.303 mmol) of $[In(S_2CNCy_2)_3]\cdot 2py$ **(2)** were dissolved separately in 10 mL each of toluene and chloroform in a round-bottomed flask connected to a deposition assembly. The reactor tube along with FTO substrate was adjusted in a tube furnace and heated upto desired temperature of 500°C for about 15 min prior to aerosols production. An ultrasonic humidifier generated the aerosols of the sample solution through

piezoelectric modulator and argon carrier gas with a flow rate 100 mL per min transported aerosols into the reactor of deposition assembly where thin layer of desired IBS composite material was produced on FTO substrate. The deposition was carried out for 40 min to get thin layer of target material. The extraction system of fuming hoods eliminated all the exhausts along with volatile by-products during the deposition experiments. After completion of depositions, the thin films were cooled to room temperature in argon gas environment before characterization and photo electrochemical studies.

Characterization of materials

The structural and topographical elucidation of synthesized IBS composite thin films were performed with field emission gun scanning electron microscope (FE-SEM, FEI Quanta 400) coupled with an energy dispersive X-ray (EDX) spectrometer (INCA Energy 200) by fixing the operational conditions at 20 kV (accelerating voltage) and 9.2 mm (working distance). The PAN analytical (X'Pert High Score) diffractometer having intense Cu-Kα radiation as X-ray source of monochromatic wavelength (λ) 1.54184 Å radiation was used to analyse phase purity of IBS films interms of crystalline phase and degree of crystallinity. In order to get all possible reflections, the target material was scanned from 10° to 90° by setting the operating parameters of the X-ray diffractometer at optimal level i.e. 0.026° (step size), 40 kV (voltage) and 40 mA (current). The Raman spectroscopy of the films was accomplished by using Raman microscope (Renishaw InVia) and 514-nm argon laser beam of intensity 0.01 mW was used to excite the samples. The X-ray photo electron spectroscopical (XPS) measurements of the composite thin film were performed on ULVAC-PHI (Quantera II) having Monochromatic X-ray source (Al Kα radiation) of energy 1486.8 eV. The carbon (C 1s) beam of energy 284.6 eV as a reference was employed for the calibration of binding energies.

The Lambda 35 Perkin-Elmer UV-vis spectrophotometer was used to measure the visible light absorption in the visible region of 350 to 900 nm using bare FTO glass substrate as reference. The surface thickness of $InBiS_3$-In_2S_3-Bi_2S_3 composite thin films was measured on KLA Tencore P-6 surface profilometer. The photoelectrochemical (PEC) measurements of the IBS thin films were carried out in a quartz window electrochemical cell consisting of 0.01 M sacrificial aqueous sodium sulphide (Na_2S) solution and thin film as working electrode, platinum wire as counter electrode and Ag/AgCl/3 M KCl as reference electrode. The PEC studies in terms of I-V curves were measured under the steady state conditions of current and voltage on a potentiostat Autolab type III (Eco Chemie micro) with cell illumination achieved by a solar simulator (AM 1.5 class A, Solar Light 16S-300) having light intensity of 100 $mWcm^{-2}$. The effective surface area of the working electrode was 1 cm^2.

Acknowledgment: This work is a part of PhD research thesis of Umar Daraz. Authors are highly thankful to the Higher Education Commission, Islamabad, Pakistan for financial support of this work under their International Research Support Initiative Programme (IRSIP). We are also greatly obliged to the Institute of Chemical Sciences, Bahauddin Zakariya University, Multan, Pakistan and the University of Malaya, Kuala Lampur, Malaysia for providing Laboratory facilities to carry out this work.

References

Ali N., Hussain A., Ahmed R., Omar M.F.B., Sultan M., Fu Y.Q., Crystallized $InBiS_3$ thin films with enhanced optoelectronic properties. Appl. Surf. Sci., 2018, 436, 293-301.

Ananthoju B., Sonia F.J., Kushwaha A., Bahadur D., Medhekar N., Aslam M., Improved structural and optical properties of Cu_2ZnSnS_4 thin films via optimized potential in single bath electrodeposition. Electrochim. Acta, 2014, 137, 154-163.

Banos R., Manzano A.F., Montoya F., Gil C., Alcayde A., Gómez J., Optimization methods applied to renewable and sustainable energy: A review. Renew. Sust. Energ. Rev., 2011, 15(4), 1753-1766.

Berengue O.M., Rodrigues A.D., Dalmaschio C.J., Lanfredi A.J., Leite E.R., Chiquito A.J., Structural characterization of indium oxide nanostructures: a Raman analysis. J. Phys. D Appl. Phys., 2010, 43(4), 045401.

Bhira L., Essaidi H., Belgacem S., Couturier G., Salardenne J., Barreaux N., et al., Structural and Photoelectrical Properties of Sprayed β-In_2S_3 Thin Films. Phys. status solidi A, 2000, 181(2), 427-435.

Calixto M., Tiburcio A., Ortiz A., Sanchez A., Optoelectronical properties of indium sulfide thin films prepared by spray pyrolysis for photovoltaic applications. Thin Solid Films, 2005, 480, 133-137.

Chen L.Y., Zhang Z.D., Wang W.Z., Self-assembled porous 3D flowerlike β-In_2S_3 structures: synthesis, characterization, and optical properties. J. Phys.Chem. C, 2008, 112(11), 4117-4123.

Chen W., Duan G.R., Liu T.Y., Jia Z.M., Liu X.H., Chen S.M., et al., Synthesis of homogeneous one-dimensional $Ni_xCd_{1-x}S$ nanorods with enhanced visible-light response by ethanediamine-assisted decomposition of complex precursors. J. Mater. Sci., 2015, 50(11), 3920-3928.

Chen X., Li L., Zhang W., Li Y., Song Q., Dong L., Fabricate Globular Flower-like $CuS/CdIn_2S_4/ZnIn_2S_4$ with High Visible Light Response via Microwave-assisted One–step Method and Its

Multipathway Photoelectron Migration Properties for Hydrogen Evolution and Pollutant Degradation. ACS Sustain. Chem. Eng., 2016, 4(12), 6680-6688.

Cheon J., Talaga D.S., Zink J.I., Laser and thermal vapor deposition of metal sulfide (NiS, PdS) films and in situ gas-phase luminescence of photofragments from M $(S_2COCHMe_2)_2$. Chem. Mater., 1997, 9(5), 1208-1212.

Dong S., Feng J., Fan M., Pi Y., Hu L., Han X., et al., Recent developments in heterogeneous photocatalytic water treatment using visible light-responsive photocatalysts: a review. RSC Adv., 2015, 5(19), 14610-14630.

Dunst S., Rath T., Reichmann A., Chien H.T., Friedel B., Trimmel G., A comparison of copper indium sulfide-polymer nanocomposite solar cells in inverted and regular device architecture. Synthetic Met., 2016, 222, 115-123.

Ehsan M.A., Peiris T. N., Wijayantha K.U., Olmstead M.M., Arifin Z., Mazhar M., et al., Development of molecular precursors for deposition of indium sulphide thin film electrodes for photoelectrochemical applications. Dalton T., 2013, 42(30), 10919-10928.

Ellabban O., Abu-Rub H., Blaabjerg F., Renewable energy resources: Current status, future prospects and their enabling technology. Renew. Sust. Energ. Rev., 2014, 39, 748-764.

Grigas J., Talik E., Lazauskas V., X-ray Photoelectron Spectra and Electronic Structure of Bi_2S_3 Crystals. phys. status solidi B, 2002, 232(2), 220-230.

Haaf S.T., Sträter H., Brüggemann R., Bauer G.H., Felser C., Jakob G., Physical vapor deposition of Bi_2S_3 as absorber material in thin film photovoltaics. Thin Solid Films, 2013, 535, 394-397.

Huang Z.F., Song J., Li K., Tahir M., Wang Y.T., Pan L., et al., Hollow cobalt-based bimetallic sulfide polyhedra for efficient all-pH-value electrochemical and photocatalytic hydrogen evolution. J. Am. Chem. Soc., 2016, 138(4), 1359-1365.

Jinlong L., Tongxiang L., Chen W., Effect of electrodeposition temperature on grain orientation and corrosion resistance of nanocrystalline pure nickel. J. Solid State Chem., 2016, 240, 109-114.

Kale R., Lokhande C., Systematic study on structural phase behavior of CdSe thin films. J. Phys. Chem. B, 2005, 109(43), 20288-20294.

Khadraoui M., Miloua R., Benramdane N., Bouzidi A., Sahraoui K., Synthesis and characterization of $(Sn_2S_3)_x(Bi_2S_3)_{1-x}$ composite thin films for solar cell applications. Mater. Chem. Phys., 2016, 169, 40-46.

Ku Y., Lin P.Y., Liu Y.C., Deposition of copper indium sulfide on TiO_2 nanotube arrays and its application for photocatalytic decomposition of gaseous IPA. Sustain. Environ. Res., 2016, 26(5), 224-229.

Kudo A., Miseki Y., Heterogeneous photocatalyst materials for water splitting. Chem. Soc. Rev., 2009, 38(1), 253-278.

Liu Z., Peng S., Xie Q., Hu Z., Yang Y., Zhang S., et al., Large Scale Synthesis of Ultralong Bi_2S_3 Nanoribbons via a Solvothermal Process. Adv. Mater., 2003, 15(11), 936-940.

Liufu S.C., Chen L.D., Yao Q., Wang C.F., Assembly of one-dimensional nanorods into Bi_2S_3 films with enhanced thermoelectric transport properties. Appl. Phys. Lett., 2007, 90(11), 112106.

Madeswaran S., Giridharan N., Jayavel R., Sol-gel synthesis and property studies of layered perovskite bismuth titanate thin films. Mater. Chem. Phys., 2003, 80(1), 23-28.

Madoun M., Baghdad R., Chebbah K., Bezzerrouk M., Michez L., Benramdane N., Temperature effect on structural and optoelectronic properties of Bi_2S_3 nanocrystalline thin films deposited by spray pyrolysis method. Mat. Sci. Semicon. Proc., 2013, 16(6), 2084-2090.

Mansoor M., Ebadi M., Mazhar M., Huang N., Mun L., Misran M., et al., Cadmium-manganese oxide composite thin films: Synthesis, characterization and photoelectrochemical properties. Mater. Chem. Phys., 2017a, 186, 286-294.

Mansoor M., Munawar K., Lim S., Huang N.M., Mazhar M., Akhtar M., et al., Iron-manganese-titanium (1: 1: 2) oxide composite thin films for improved photocurrent efficiency. New J. Chem., 2017b, 41(15), 7322-7330.

Mansoor M.A., Mazhar M., McKee V., Arifin Z., Mn_2O_3–$4TiO_2$ semiconducting composite thin films for photo-electrochemical water splitting. Polyhedron, 2014, 75, 135-140.

Marchand P., Hassan I.A., Parkin I. P., Carmalt C.J., Aerosol-assisted delivery of precursors for chemical vapour deposition: expanding the scope of CVD for materials fabrication. Dalton T., 2013, 42(26), 9406-9422.

Moreno H.G., Nair M., Nair P., Chemically deposited lead sulfide and bismuth sulfide thin films and Bi_2S_3/PbS solar cells. Thin Solid Films, 2011, 519(7), 2287-2295.

Munawar K., Mansoor M.A., Basirun W. J., Misran M., Huang N.M., Mazhar M., Single step fabrication of CuO-MnO-$2TiO_2$ composite thin films with improved photoelectrochemical response. RSC Adv., 2017, 7(26), 15885-15893.

Nagesha D.K., Liang X., Mamedov A.A., Gainer G., Eastman M.A., Giersig, M., et al., In_2S_3 nanocolloids with excitonic emission: In_2S_3 vs CdS comparative study of optical and structural characteristics. J. Phys. Chem. B, 2001, 105(31), 7490-7498.

Ning X., Li J., Yang B., Zhen W., Li Z., Tian B., et al., Inhibition of photocorrosion of CdS via assembling with thin film TiO_2 and removing formed oxygen by artificial gill for visible light overall water splitting. Appl. Catal. B-Environ., 2017, 212, 129-139.

Ota J., Srivastava S.K., Polypyrrole coating of tartaric acid-assisted synthesized Bi_2S_3 nanorods. J. Phys. Chem. C, 2007, 111(33), 12260-12264.

Pathak A., The growth of bismuth sulfide nanorods from spherical-shaped amorphous precursor particles under hydrothermal condition. J. Nanopart., 2013, 2013.

Pineda E., Nicho M.E., Nair P., Hu H., Optoelectronic properties of chemically deposited Bi_2S_3 thin films and the photovoltaic performance of Bi_2S_3/P_3OT solar cells. Sol. Energy, 2012, 86(4), 1017-1022.

Primo A., Corma A., García H., Titania supported gold nanoparticles as photocatalyst. Phys. Chem. Chem. Phys., 2011, 13(3), 886-910.

Protti S., Albini A., Serpone N., (2014). Photocatalytic generation of solar fuels from the reduction of H_2O and CO_2: a look at the patent literature. Phys. Chem. Chem. Phys., 2014, 16(37), 19790-19827.

Rabin O., Perez J.M., Grimm J., Wojtkiewicz G., Weissleder R., An X-ray computed tomography imaging agent based on long-circulating bismuth sulphide nanoparticles. Nat. Mater., 2006, 5(2), 118.

Sankir N.D., Aydin E., Ugur E., Sankir M., Non-toxic and environmentally friendly route for preparation of copper indium sulfide based thin film solar cells. J. Alloy. Compd., 2015, 640, 468-474.

Shen J., Zai J., Yuan Y., Qian X., 3D hierarchical $ZnIn_2S_4$: the preparation and photocatalytic properties on water splitting. Int. J. of Hydrogen Energ., 2012, 37(22), 16986-16993.

Spasevska H., Kitts C.C., Ancora C., Ruani G., Optimised In_2S_3 thin films deposited by spray pyrolysis. Int. J. Photoenergy, 2012, 2012.

Sterner J., Malmström J., Stolt L., Study on ALD In_2S_3/Cu(In,Ga)Se_2 interface formation. Prog. Photovoltaics Res. Appl., 2005, 13(3), 179-193.

Tahir A.A., Ehsan M.A., Mazhar M., Wijayantha K.U., Zeller M., Hunter A., Photoelectrochemical and photoresponsive properties of Bi_2S_3 nanotube and nanoparticle thin films. Chem. Mater., 2010, 22(17), 5084-5092.

Tong H., Ouyang S., Bi Y., Umezawa N., Oshikiri M., Ye J., Nano-photocatalytic materials: possibilities and challenges. Adv. Mater., 2012, 24(2), 229-251.

Tsuji I., Kato H., Kudo A., Visible-Light-Induced H_2 Evolution from an Aqueous Solution Containing Sulfide and Sulfite over a ZnS–$CuInS_2$–$AgInS_2$ Solid-Solution Photocatalyst. Angew. Chem. Int. Edit., 2005, 44(23), 3565-3568.

Wang C.C., Li J.R., Lv X.L., Zhang Y.Q., Guo G., Photocatalytic organic pollutants degradation in metal–organic frameworks. Energy Environ. Sci., 2014 7(9), 2831-2867.

Weide P., Schulz K., Kaluza S., Rohe M., Beranek R., Muhler M., Controlling the photocorrosion of zinc sulfide nanoparticles in water by doping with chloride and cobalt ions. Langmuir, 2016, 32(48), 12641-12649.

Yadav A.A., Salunke S., Photoelectrochemical properties of In_2Se_3 thin films: Effect of substrate temperature. J. Alloy. Compd., 2015, 640, 534-539.

Yang B., Wang L., Han J., Zhou Y., Song H., Chen S., et al., $CuSbS_2$ as a promising earth-abundant photovoltaic absorber material: a combined theoretical and experimental study. Chem. Mater., 2014, 26(10), 3135-3143.

Zhang K., Guo L., Metal sulphide semiconductors for photocatalytic hydrogen production. Catal. Sci. Technol., 2013, 3(7), 1672-1690.

Zou X., Liu Y., Li G.D., Wu Y., Liu D.P., Li W., et al., Ultrafast Formation of Amorphous Bimetallic Hydroxide Films on 3D Conductive Sulfide Nanoarrays for Large-Current-Density Oxygen Evolution Electrocatalysis. Adv. Mater., 2017, 29(22).

Zumeta I.D, Ortiz J.L., Díaz D., Trallero C., Ruiz V.F., First order raman scattering in bulk Bi_2S_3 and quantum dots: Reconsidering controversial interpretations. J. Phys. Chem. C, 2014, 118(51), 30244-30252.